Radio Science, Volume ???, Number , Pages 1?? ,

Generation of artificial ULF/ELF electromagnetic emission in the ionosphere by horizontal ground-based current system

E. N. Fedorov[1], N. G. Mazur[1], and V. A. Pilipenko[1,2]

[1] *Institute of Physics of the Earth, B. Gruzinskaya 10, Moscow 123995, Russia*

[2] *Geophysical Center, Molodeznaya 3, Moscow 119296, Russia*

Corresponding author: V.A. Pilipenko

Keypoints

- Numerical model of ULF/ELF emission generation in the ionosphere by a near-ground linear current of finite length has been elaborated
- Electromagnetic 50-Hz field emitted by 100 km current source is ∼3.7 times less than that predicted by the infinite line model
- Artificial ULF/ELF emissions can be launched into the upper ionosphere by ground-based large-scale current systems

Abstract. The feasibility of detection of electromagnetic response in the upper ionosphere to ground large-scale ultra-low-frequency (ULF) and extremely-low-frequency (ELF) transmitters by low-Earth orbit (LEO) satellites is considered. As an example of such transmitters, we consider the ZEVS 82 Hz transmitter for submarine communication, FENICS experiments with decommissioned electric power lines driven by 0.5–150 Hz generator, and industrial 50 Hz power transmission lines. We numerically model the ULF/ELF wave energy leakage into the upper ionosphere from an oscillating grounded linear current of a finite

length suspended above a high-resistive ground. A realistic altitudinal profile of the plasma parameters has been reconstructed with the use of the IRI ionospheric model. For the ZEVS transmitter powered by 200 A current the modeled amplitudes of electromagnetic response can reach in the upper nightside ionosphere up to 60 μV/m and 6 pT. The assumption of an infinite source scale overestimates the ionospheric response by a factor of $\sim$6 as compared with realistic scale 60 km of the ZEVS transmitter. Unbalanced 50 Hz current of 10 A in large-scale ($>$ 100 km) power transmission lines can produce the electric response in the upper ionosphere that is sufficient to be detected by electric sensors at LEO satellite. The stimulation of artificial Pc1 pulsations (0.5 Hz) with amplitudes $\sim$ 1 pT and $\sim$ 10 μV/m by large-scale decommissioned power lines is possible with driving current $>$ 100 A.

Plain Language Summary

Our planet was found to exist in an electromagnetic environment, at least in some frequency bands, created by rather industrial activity than by natural processes. The electromagnetic response in the ionosphere to thunderstorms and radio transmitters has been well studied in the VLF frequency range ($>$ 1 kHz), but much less attention has been paid to the ULF ($<$ 1 Hz) and ELF ($<$ 1 kHz) bands. Any noticeable ULF/ELF emission efficiency may be expected only for extremely large-scale emitting systems. Such man-made transmitters do exist. Powerful ELF aerials for communication with submarines with a length about several tens of km were constructed. Special experiments with controlled sources of electromagnetic fields of ULF/ELF bands were carried out using decommissioned power lines as a horizontal radiating antenna. Transportation systems can also be an extended

ULF antenna. Finally, unbalanced networks of electric power transmission 50/60 Hz lines become large-scale emitters. Our numerical modeling has proved that manmade ULF/ELF electromagnetic activity near the ground can be monitored by LEO satellites. The large-scale decommissioned power lines can be used to stimulate artificial Pc1 pulsations with frequency ≤ 1 Hz in the ionosphere-magnetosphere system.

Keywords: ULF waves, ELF emission, power line emission, power transmission lines, ionospheric signals

1. Introduction: Large-scale ELF transmitters

There appear ever growing evidences of man-made influence on natural processes in the near-Earth space [*Parrot*, 2018]. This influence was found not only in dedicated active experiments, but also as unintentional by-product of the technosphere development [*Rothkaehl & Parrot*, 2005]. The electromagnetic response in the ionosphere to natural (e.g., thunderstorms) [*Inan et al.*, 2010] and man-made (e.g., radio transmitters) [*Starks et al.*, 2002] sources has been well studied in the very-low-frequency (VLF) range (> 1 kHz). Much less attention has been paid to the ultra-low-frequency (ULF) range (below fundamental Schumann resonance $\sim$8 Hz) and the extra-low-frequency (ELF) range (above the Schumann resonance, but $<<1$ kHz). Any noticeable ULF/ELF emission efficiency may be expected only from an extremely large-scale emitting system. Such man-made transmitters do exist. Powerful aerials for communication with submarines with a length about several tens of km have been constructed in various countries [*Bannister et al.*, 1992]. In particular, the transmitter ZEVS operates near the coastline of White Sea. Controlled sources of electromagnetic

fields in ULF/ELF bands using decommissioned power lines as a horizontal radiating antenna were applied for deep magnetotelluric (MT) sounding of the lithosphere [*Boerner*, 1992; *Velikhov et al.*, 1994]. All industrial regions of the Earth are covered by networks of electric power transmission 50/60 Hz lines extended to many hundreds of km. If the transmitted currents are unbalanced by some reason, these power lines become large-scale emitters. Rail transportation systems also can be the source of ULF/ELF electromagnetic disturbances. For example, power for trains in California is provided by a 1000 V rail with total length 270 km. Large fluctuating currents (5-10 kA) that flow in this rail make the entire train system a large ULF antenna [*Fraser-Smith & Coates*, 2022].

Electromagnetic disturbances and emissions from large-scale systems can be observed at vast territories and even leak into the outer space. The most ubiquitous type of electromagnetic radiation emanating from the Earth is the 50/60 Hz power line emission (PLE). PLEs were discovered in the upper ionosphere at the fundamental frequency and its third harmonic above highly industrialized regions in low-Earth-orbit (LEO) satellite missions [*Zhang & Ma*, 2018; *Pilipenko et al.*, 2021]. The PLE intensities recorded during magnetically disturbed periods were systematically larger than the intensities observed during low magnetic activity, and the nighttime overall intensities were considerably larger than the day time intensities [*Nemec et al.*, 2015]. The DEMETER satellite observations revealed that an amount of global emitted energy by transmission lines has been ever increasing in time since the world total electric generation power increases. A sudden increase in number of PLE events observed in space was especially noticeable since extra-high-voltage (EHV) and ultra-high-voltage (UHV) transmission projects started to develop rapidly [*Wu et al.*,

2019a]. Geographic maps of the PLE occurrence rates recorded by DEMETER satellite showed remarkable agreement with the world map of power consumption [*Nemec et al.*, 2015]. Power lines can be an effective emitter not only of 50/60 Hz PLE, but power line harmonic radiation (PLHR) at very high harmonics, about 1 kHz [*Nemec et al.*, 2008; *Wu et al.*, 2019a]. In this frequency range a power line can operate as a Beverage antenna [*Kostrov et al.*, 2017]. This explains a ubiquity of PLHR observations in space.

The 82 Hz emission was detected by the DEMETER satellite during overflights above the ZEVS transmitter [*Parrot*, 2018; *Pilipenko et al.*, 2019]. No attempt to detect ULF/ELF emissions in space during experiments with controlled MT sources were performed yet.

Electromagnetic field propagation along the Earth surface from an ELF emitting dipole in the Earth-ionosphere waveguide has been well modeled [*Bernstain et al.*, 1974; *Tereshenko & Tereshenko*, 2017; *Nickolaenko et al.*, 2016; *Sobchakov et al.*, 2003]. In these works the ionosphere is modeled as a conductive homogeneous layer because the wave leakage into the ionosphere is small and such simplified models are quite adequate for the description of ELF wave long-distance propagation in the waveguide Earth - bottom ionosphere. Besides submarine communication, a great stimulus for such studies was provided by experiments with controlled sources of electromagnetic fields of ULF/ELF bands using decommissioned power lines as a horizontal radiating antenna [*Zhamaletdinov et al.*, 2015]. The artificial ULF-ELF signals were detected at large distances from the emitter [*Belyaev et al.*, 2002; *Ermakova et al.*, 2006].

At the same time, the ULF/ELF wave energy transmission from ground sources towards LEO has not been adequately examined with a realistic ionospheric model. In contrast to

VLF emitters (like radio transmitters or lightning strokes) a source of ULF/ELF emissions cannot be modeled as a point dipole, but its finite scale, often exceeding the height of the lower ionosphere (∼100 km), must be taken into an account. As a first step, *Fedorov et al.* [2020] presented a numerical model of electromagnetic response of a realistic ionosphere in the vertical geomagnetic field $\mathbf{B}_0$ to a near-ground infinite linear current. This theoretical model was advanced in [*Fedorov et al.*, 2021] by consideration of arbitrary geomagnetic field inclination and power line orientation. The account for a geomagnetic field inclination makes the problem significantly more complicated because the medium parameters become axially non-symmetric. The elaborated numerical model for realistic mid-latitude ionosphere with inclined $\mathbf{B}_0$ showed that PLE energy is partially guided by geomagnetic field lines, so the maximal intensity in the upper ionosphere is shifted equatorward from a vertical and diminishes upon the latitude decrease, but not significantly.

In this paper we further investigate theoretically the efficiency of the ULF/ELF wave excitation in the upper ionosphere by a linear near-Earth grounded current of a finite length. The mathematical basis for this numerical model has been elaborated in [*Fedorov et al.*, 2022]. On the basis of this mathematical formalism, we have elaborated a numerical model with a realistic ionospheric profile. A special attention has been paid to the dependence of a maximal emission intensity on the length of a near-ground emitter. The expected wave amplitude at LEO for various types of ELF transmitters has been calculated.

2. Possible ELF sources

Oppositely to standard radio transmitters, the generation of artificial signals in the ULF-ELF range needs specific large-scale devices to be efficient. To communicate with submarines below water and ice, the Russian Navy deployed the ELF transmitter ZEVS on the Kola peninsula. ZEVS consists of two parallel horizontal grounded antennas about 60 km in length that emit at frequency 82 Hz [*Velikhov et al.*, 1998]. The transmitter lines are elongated nearly in the East-West direction at the latitude $68^0 48'$ N. The generator pumps in the antenna a current up to 200-300 A and power up to 2.5 MW.

The experiments FENICS (Fennoscandian Electrical conductivity from soundings with the Natural and Controlled Sources) are conducted regularly at Kola Peninsula with the use of two decommissioned power transmission lines with length $L = 100$ km and $L = 120$ km as controlled ULF-ELF emitters [*Zhamaletdinov et al.*, 2015]. During the experiments the generator with power 200 kW yields in power lines the alternating current (AC) with amplitude from 240 A at low frequencies (< 10 Hz) to 20 A at higher frequencies (~ 200 Hz).

Under ideal conditions, a three-phase power transmission line must be balanced (symmetrical) when the voltages and currents of each phases have the same amplitude and phase shift of 120°. If at least one of these conditions is not met, then the system becomes unbalanced. Such imbalance leads to a decrease in the efficiency of a transmission line and power losses due to the radiation of electromagnetic energy. In most cases, the source of the imbalance is the asymmetry of the load (high-speed railways, metallurgy induction furnaces, computer centers, etc.). Substantial distortions in the power line operation can be produced by geomagnetically induced currents (GICs) caused by rapid variations of the geomagnetic

field, i.e. high dB/dt values (see review [*Pilipenko et al.*, 2021]). The detection of PLE at large distances from a three-phase power line is an indicator of its unbalanced operation.

3. Modeling the electromagnetic field of a horizontal line current above a conducting ground

The developed numerical model considers the multi-layered horizontally homogeneous medium with a realistic ionospheric vertical profile. The model of the medium is like the model used for the description of ULF transients in the ionosphere produced by lightning discharges [*Fedorov et al.*, 2016; *Mazur et al.*, 2018], whereas the sources, basic equations, and solution technique are different.

We consider electromagnetic field only in the vicinity of the transmitter (about several hundred km and less). For such distances the plane geometry is a good approximation. The axis Z of the Cartesian coordinate system is chosen to be vertical upward with $z = 0$ on the ground, whereas X is eastward, and Y is northward. For simplicity the geomagnetic field is assumed to be vertical (the inclination of geomagnetic field $I = 90°$). We assume that the electromagnetic field is excited by a linear current $J(t) = J_0 \exp(-i\omega t)$ along axis X, situated at altitude h above the Earth's surface and oscillating with frequency ω. However, in contrast with previous studies, the length of emitting line L is considered as finite one.

Upon modeling of the grounded linear current suspended above the Earth surface, it is necessary to take into account the spreading electric currents inside the Earth. The easiest way to do this is to shift formally the current downward into the Earth to a small depth (about few meters). This small downward shift of the antenna has no effect on the field

in the atmosphere and ionosphere but reduces the problem to a much simpler geometrical consideration.

We search magnetic $\mathbf{B}(x,y,z,t)$ and electric $\mathbf{e}(x,y,z,t) \equiv c^{-1}\mathbf{E}$ fields (c is light velocity) as a time harmonic $\propto \exp(-i\omega t)$, and solve Maxwell′s equations with the external driving current density $\mathbf{j}$

$$\boldsymbol{\nabla} \times \mathbf{B} = -ik_0\hat{\boldsymbol{\varepsilon}}\mathbf{e} + \mu_0\mathbf{j}, \qquad \boldsymbol{\nabla} \times \mathbf{e} = ik_0\mathbf{B}, \tag{1}$$

Here $k_0 = \omega/c$ is the wave number in a free space, and the tensor of relative dielectric permeability of the ionospheric plasma $\hat{\boldsymbol{\varepsilon}} = \boldsymbol{\varepsilon}/\varepsilon_0$ (where ε_0 is the vacuum dielectric permeability) in the field-aligned coordinate system has the form

$$\hat{\boldsymbol{\varepsilon}} = \begin{pmatrix} \varepsilon_\perp & ig & 0 \\ -ig & \varepsilon_\perp & 0 \\ 0 & 0 & \varepsilon_\parallel \end{pmatrix}.$$

The standard formulas for the elements of the tensor $\boldsymbol{\varepsilon}$ in a collisional plasma can be found elsewhere (e.g., [*Wait*, 1972]). In the near-Earth atmosphere the tensor elements are reduced to $\varepsilon_\perp = \varepsilon_\parallel \to 1$ and $g \to 0$.

The first step in solving the problem is to find a solution of Maxwell′s equations with a source as a point horizontal current (current dipole). This formalism is detailed below in subsection 3.2, where the specific form of Maxwell's equations is given for this particular case. Having found a solution for such an elementary source, at the next step it is easy to calculate the total field, excited by a horizontal current of finite length, just summarizing the fields generated by elementary current dipoles.

3.1. Equations for the wave potentials

We use the representation of electromagnetic field via the wave potentials. In this formalism the field can be split into the potential and vortex (eddy) components. This division is fundamental in solving the given problem. The initial problem is obviously devoid of axial symmetry, while it turns out that the potential and vortex components separately have such symmetry. Thanks to this, it becomes possible to separate variables using the Hankel′s transform and come to a boundary problem for a system of ordinary differential equations (ODEs).

The electric and magnetic fields are standardly represented using scalar Φ and vector $\mathbf{A}$ potentials as follows $\mathbf{B} = \boldsymbol{\nabla} \times \mathbf{A}$ and $\mathbf{e} = -\boldsymbol{\nabla}\Phi + ik_0\mathbf{A}$. The total field can be represented as a sum of coupled partial electric (A) and magnetic (F) modes. In the MHD limit, the partial electric mode corresponds to the Alfven wave, whereas the partial magnetic mode corresponds to the fast magnetosonic wave. In general, the electric and magnetic modes are determined by the scalar potential Φ and the longitudinal component of the vector potential $A \equiv A_z$ and the transverse vector potential $\mathbf{A}_\perp$, correspondingly,

$$\mathbf{B}_A = \boldsymbol{\nabla} \times A\hat{\mathbf{z}}, \quad \mathbf{e}_A = -\boldsymbol{\nabla}\Phi + ik_0 A\hat{\mathbf{z}}. \tag{2}$$

$$\mathbf{B}_F = \boldsymbol{\nabla} \times \mathbf{A}_\perp, \quad \mathbf{e}_F = ik_0\mathbf{A}_\perp. \tag{3}$$

The potential $\mathbf{A}_\perp$ is related to the magnetic potential Ψ as follows: $\mathbf{A}_\perp = (ik_0)^{-1}\boldsymbol{\nabla} \times \Psi\hat{\mathbf{z}}$. Using the relationships (3), the expressions for the total field via the potentials A, Φ, and

Ψ can be found:

$$\mathbf{B} = \mathbf{B}_A + \mathbf{B}_F = \boldsymbol{\nabla} A \times \hat{\mathbf{z}} + (ik_0)^{-1}\boldsymbol{\nabla}_\perp \partial_z \Psi - (ik_0)^{-1}\nabla_\perp^2 \Psi \hat{\mathbf{z}}, \tag{4}$$

$$\mathbf{e} = \mathbf{e}_A + \mathbf{e}_F = -\boldsymbol{\nabla}\Phi + ik_0 A\hat{\mathbf{z}} + \boldsymbol{\nabla}\Psi \times \hat{\mathbf{z}}. \tag{5}$$

From Maxwell′s equations (1) and expressions (5) the system of equations describing these potentials follows [*Fedorov et al.*, 2022]

$$\begin{gathered}
\nabla_\perp^2 \partial_z A = ik_0 \varepsilon_\perp \nabla_\perp^2 \Phi + k_0 g \nabla_\perp^2 \Psi + \mu_0 \operatorname{Div} \mathbf{j}_\perp , \\
\nabla_\perp^2 (\partial_z^2 + \nabla_\perp^2 + k_0^2 \varepsilon_\perp)\Psi = -ik_0^2 g \nabla_\perp^2 \Phi + ik_0 \mu_0 \operatorname{Curl} \mathbf{j}_\perp , \\
\partial_z \Phi = ik_0[1 + (k_0^2 \varepsilon_\parallel)^{-1}\nabla_\perp^2]A - (ik_0\varepsilon_\parallel)^{-1}\mu_0 j_\parallel .
\end{gathered} \tag{6}$$

Here 2D differential operators $\operatorname{Div}\mathbf{a} = \boldsymbol{\nabla}_\perp \cdot \mathbf{a} = \partial_x a_x + \partial_y a_y$ and $\operatorname{Curl}\mathbf{a} = (\boldsymbol{\nabla} \times \mathbf{a})_z = \partial_x a_y - \partial_y a_x$ have been used.

3.2. Field of a point horizontal current

Now we study the field produced by a horizontal current with magnitude J_0 and length d which is much less than the distance to the observation point. Such an elementary source may be considered as a current dipole with the moment $M_0 = J_0 d$, which is located at height $z = h$ and directed along the axis X. For such source the driver current density in (6) has the components $j_\parallel = 0$, and $\mathbf{j}_\perp = j_x(\varrho, z)\hat{\mathbf{x}} = M_0(2\pi\varrho)^{-1}\delta(\varrho)\delta(z-h)\hat{\mathbf{x}}$, in the cylindrical coordinates ϱ, φ, z. Thus, the source terms in (6) for current dipole case are as follows

$$\operatorname{Div}\mathbf{j}_\perp = q(\varrho)\delta(z-h)\cos\varphi, \quad \operatorname{Curl}\mathbf{j}_\perp = -q(\varrho)\delta(z-h)\sin\varphi, \quad q(\varrho) = M_0\partial_\varrho[(2\pi\varrho)^{-1}\delta(\varrho)]. \tag{7}$$

The $\operatorname{Div}\mathbf{j}_\perp$ term produces the potential part of a field excited by the current dipole, while the $\operatorname{Curl}\mathbf{j}_\perp$ term produces the vortex part. Thus, the angular φ-dependence of the driver terms is closely connected to the vorticity of the excited field. The solution of the system (6) with

such specific form of driver terms is searched as $F(\varrho,\varphi,z) = F_c(\varrho,z)\cos\varphi + F_s(\varrho,z)\sin\varphi$, where $F = A,\Phi,\Psi$. Substituting these combinations into (6) and grouping terms with factors $\cos\varphi$ and $\sin\varphi$, the following system is obtained [*Fedorov et al.*, 2022]

$$\begin{array}{l} \partial_z A_{c,s} = ik_0\varepsilon_\perp \Phi_{c,s} + k_0 g \Psi_{c,s} + a_{c,s} \\ \partial_z B_{c,s} = -k_0 g \Phi_{c,s} - (ik_0)^{-1}(k_0^2\varepsilon_\perp + \mathrm{R})\Psi_{c,s} - b_{c,s} \\ \partial_z \Phi_{c,s} = ik_0[1 + (k_0^2\varepsilon_\parallel)^{-1}\mathrm{R}]A_{c,s} \\ \partial_z \Psi_{c,s} = ik_0 B_{c,s} \end{array} \tag{8}$$

Here the operator $\mathrm{R} = \varrho^{-1}\partial_\varrho\varrho\partial_\varrho - \varrho^{-2}$, the inhomogeneous terms are $a_c = b_s = \mu_0\mathrm{R}^{-1}q(\varrho)\delta(z-h)$ and $a_s = b_c = 0$. For symmetry the additional function $B_{c,s} = (ik_0)^{-1}\partial_z\Psi_{c,s}$ has been introduced.

Of fundamental importance is the fact that the system (8) has a cylindrical symmetry, thus the asymmetry of the original problem has been overcome thanks to splitting into two components having different angular dependence ($\propto\cos\varphi$ and $\propto\sin\varphi$). This gives a possibility to separate variables and arrive at 1D boundary value problem. The system (8) of partial differential equations is further reduced to the system of ODEs in respect to the variable z using the Hankel′s transform of the 1-st order. This transform $\mathbb{K}_1[f(\varrho)](k)$ reduces the differential operator R to simple multiplication by $-k^2$. Applying the transform $\mathbb{K}_1$ to (8) and introducing new variables $\tilde{A}_{c,s} = k\mathbb{K}_1[A_{c,s}]$, $\tilde{B}_{c,s} = k\mathbb{K}_1[B_{c,s}]$, $\tilde{\Phi}_{c,s} = k\mathbb{K}_1[\Phi_{c,s}]$, and $\tilde{\Psi}_{c,s} = k\mathbb{K}_1[\Psi_{c,s}]$, we arrive at the system of ODEs

$$\begin{array}{ll} \partial_z\tilde{A}_{c,s} = \alpha\tilde{\Phi}_{c,s} + \beta\tilde{\Psi}_{c,s} + \tilde{a}_{c,s}\,, & \partial_z\tilde{\Phi}_{c,s} = \lambda\tilde{A}_{c,s}\,, \\ \partial_z\tilde{B}_{c,s} = \gamma\tilde{\Phi}_{c,s} + \delta\tilde{\Psi}_{c,s} - \tilde{b}_{c,s}\,, & \partial_z\tilde{\Psi}_{c,s} = ik_0\tilde{B}_{c,s}\,. \end{array} \tag{9}$$

Here $\alpha = ik_0\varepsilon_\perp$, $\beta = k_0 g$, $\gamma = -k_0 g$, $\delta = ik_0(\varepsilon_\perp - k^2/k_0^2)$, $\lambda = ik_0[1 - k^2/(k_0^2\varepsilon_\parallel)]$, $\tilde{a}_c = \tilde{b}_s = (2\pi)^{-1}\mu_0 M_0\delta(z-h)$, and $\tilde{a}_s = \tilde{b}_c = 0$. The system (9) is augmented with boundary conditions at $z \to \pm\infty$. It is natural to assume that electromagnetic field decreases upon an uplift into the ionosphere and immersion into the Earth. The numerical solution scheme

of the boundary problem under consideration for the system (9) was described in detail in [*Fedorov et al.*, 2022], so here just a short outlook of this procedure is given.

The occurrence of the factor $\delta(z-h)$ in the inhomogeneous terms of the system (9) makes it equivalent to a homogeneous system with matching condition at $z = h$. This condition can be obtained by integration of (9) from $z = h - 0$ to $z = h + 0$. The variables $\tilde{\Phi}_{c,s}(z)$ and $\tilde{\Psi}_{c,s}(z)$ are continuous at $z = h$, while the variables $\tilde{A}_{c,s}(z)$ and $\tilde{B}_{c,s}(z)$ have there a discontinuity. The homogeneous system can be presented symbolically as

$$\partial_z \mathbf{u} = \mathbf{S}\mathbf{v}, \qquad \partial_z \mathbf{v} = \mathbf{T}\mathbf{u}, \tag{10}$$

using 2D vectors $\mathbf{u} = (\tilde{A}_{c,s}, \tilde{B}_{c,s})$, $\mathbf{v} = (\tilde{\Phi}_{c,s}, \tilde{\Psi}_{c,s})$, and 2×2 matrices $\mathbf{S}$ and $\mathbf{T}$ of the coefficients in (9).

It is helpful to introduce the matrix $\mathbf{Y}(z)$, which transforms the vector $\mathbf{v}(z)$ into the vector $\mathbf{u}(z)$ as follows: $\mathbf{u}(z) = \mathbf{Y}(z)\mathbf{v}(z)$. This matrix is similar to the impedance matrix relating electric and magnetic components [*Budden*, 1985]. Introduction of the impedance matrix facilitates the solution of Maxwell′s equations upon appearance of fast growing and decaying wave modes. The matrix $\mathbf{Y}(z)$ obeys the nonlinear differential equation of the Riccati type $\partial_z \mathbf{Y} = \mathbf{S} - \mathbf{Y}\mathbf{T}\mathbf{Y}$. The boundary conditions for the system (9) determine unambiguously the limiting values of the matrix $\mathbf{Y}$ at $z \to \pm\infty$. Therefore, one can calculate $\mathbf{Y}(z)$ by numerical solution of this Riccati equation from above and from below to the source location and obtain different values $\mathbf{Y}(h \pm 0)$ there. Combining this discontinuity with matching conditions at the source altitude $z = h$ for the system (10) one can find the limiting values of the vectors $\mathbf{u}(h \pm 0)$ and $\mathbf{v}(h \pm 0)$. Using them as the boundary values for a numerical solution of Cauchy problem for the system (10) upwards and downwards from the source level we get

a solution of (9) at any height z. Finally, when the solution of the system (9) has been obtained, we apply to it the inverse Hankel′s transform and use the relationships (5) for the field components via the potentials, thus arriving at the results presented in Appendix.

3.3. Field of the finite-length current

Let a line current with amplitude J_0 and length L be situated at the segment $-L/2 \leq x \leq L/2$. To find the electromagnetic field generated by this finite-length current we use the results for a current dipole (see Appendix). Let us set a large number N of such elementary dipoles with the moment $M_0 = J_0 d$ to the middles of N subsegments, namely to the points $x_n = -L/2 - d/2 + nd \;\; (n = 1, \ldots, N)$, where $d = L/N$. The total current corresponding to such system of dipoles is $J_0 = NM_0 L^{-1}$. A discrete structure of such system of elementary currents Reveals itself only at small distances $\leq d$.

The calculation of the fields $\mathbf{B}(x, y, z)$ and $\mathbf{e}(x, y, z)$ produced by this set of horizontal current dipoles is illustrated in Figure 1. The cylindrical coordinates $\varrho_n(x, y)$ and $\varphi_n(x, y)$ of the observation point (x, y, z) with respect to n-th dipole are $\varrho_n = [(x - x_n)^2 + y^2]^{1/2}$ and $\varphi_n = \arcsin(y\varrho_n^{-1})$. Substituting these values into the formulas from the Appendix, we obtain the horizontal components of the field produced by n-th dipole: $B^{(n)}_{\varrho,\varphi}(x, y, z) = B_{\varrho,\varphi}(\varrho_n, \varphi_n, z)$ and $e^{(n)}_{\varrho,\varphi}(x, y, z) = e_{\varrho,\varphi}(\varrho_n, \varphi_n, z)$. These components are to be transformed by the corresponding rotation to the fixed coordinate system with axes X, Y: $B^{(n)}_{\varrho,\varphi}(x, y, z) \to B^{(n)}_{x,y}(x, y, z)$ and $e^{(n)}_{\varrho,\varphi}(x, y, z) \to e^{(n)}_{x,y}(x, y, z)$. Finally, these fields from all dipoles are summed up to determine the total field generated by the finite-length line current.

4. Modeling the electromagnetic emission produced by grounded ELF transmitter

The ionospheric reference ionosphere (IRI) is the most validated and widespread model of a regular ionosphere, which provides for any location on Earth and time moment the vertical profile of main ionospheric constituents (https://irimodel.org). The IRI parameters have been chosen, rather arbitrary, to correspond to winter nighttime conditions (LT=21, 2007/12/08) and geographic latitude 69° corresponding to the ZEVS/FENICS location. The IRI-derived static Pedersen and Hall conductances are $\Sigma_P = 0.04$ S, $\Sigma_H = 0.12$ S; the density peak height is $h_mF2 = 303$ km, and the total ionospheric content (integration from 50 to 2000 km) is 0.5 TECu. The ZEVS/FENICS installations are located at a crystalline shield with a high resistance $\sim 10^5$ Ohm·m. The atmospheric conductivity is taken to be $\sigma_a = 1.1 \cdot 10^{-14}$ S/m near the ground surface and increases exponentially to the altitude of 80 km to match the IRI-deduced conductivity. According to the IGRF geomagnetic model, the magnetic field inclination at the ZEVS/FENICS location is $I = 78°$. Because the distinction from the vertical magnetic field is small, we assume that $I = 90°$. The same ionospheric and geoelectric parameters are used for the modeling of power transmission lines.

The calculated field components are normalized to the source current $J_0 = 1$ A. The excited field is estimated at fixed altitude ($z = 660$ km) corresponding to the DEMETER orbit.

4.1. ZEVS transmitter

In earlier papers [*Fedorov et al.*, 2020; *Pilipenko et al.*, 2019] the source current was supposed to be infinitely long. This assumption probably overestimated the effect from a

realistic current with a finite length 60 km, but how severely? To answer this question, we have calculated the electric field in the upper ionosphere excited by the grounded emitters with $f = 82$ Hz and different lengths (Figure 2). For a very large-scale source $L = 5000$ km (such extended current practically corresponds to the model with infinite line) the normalized total amplitude of transverse electric field $|\mathbf{E}|$ reaches above the source ($\rho = 0$) the magnitude ~ 2.9 μV/m. For the emitter with scale 60 km, the amplitude decreases down to ~ 0.5 μV/m. Thus, the assumption of an infinite scale overestimates the E-field in the upper ionosphere by a factor of ~ 6 as compared with realistic scale ($L = 60$ km) of the ZEVS transmitter. The field decrease from a source is rather slow, so upon separation by 200 km from the vertical above the source, the amplitude drops 2.8 times only. At larger distances ($\rho > 200$ km), the difference between the infinite and finite-scale currents becomes not very significant.

The normalized total transverse magnetic field $|\mathbf{B}|$ in the upper ionosphere can reach up to $\sim$0.05 pT for the emitting current with $L = 60$ km (Figure 3). The spatial structure of magnetic disturbance nearly repeats that of electric disturbance.

The radiation pattern of the excited E-field in various directions, measured by the angle φ, is shown in Figure 4. Above the source ($\rho = 20$ km) the radiation is nearly isotropic. Away from the source ($\rho = 120$ km) the largest $|\mathbf{E}|$ field is observed in the middle of quadrant (at $\varphi \simeq 45°$), where $|E_x| \approx |E_y|$. Upon further increase of ρ, ($\rho = 240$ km) the emission becomes nearly isotropic again. Thus, though the source is linear the emission transmitted into the ionosphere is nearly circular.

According to the modeling results, the ZEVS transmitter with scale 60 km and $J_0 = 200$ A can produce the response in the upper nightside ionosphere up to 60 μV/m and 6 pT. Such amplitudes can be detected by LEO satellite. Indeed, DEMETER satellite recorded 82-Hz emission from transmitter ZEVS with amplitude 3–100 μV/m under various conditions [*Pilipenko et al.*, 2019]. Figure 2 provides a possibility to estimate the radius of a spot in the ionosphere where the emission can be detected by a satellite sensor. For that the sensitivity of the satellite instrument should be given.

4.2. FENICS installation

Now we consider the ULF/ELF emission intensity that may be observed in the upper ionosphere ($z = 660$ km) above the FENICS installation (L=100 km). The normalized emission intensity $|E|$ from transmitter with $J_0 = 1$ A for various emission frequencies is shown in Figure 5. Just above the FENICS installation ($\rho = 0$) the wave transmission into the ionosphere becomes better with increase of frequency: upon increase of f from 0.5 Hz to 150 Hz the E-field increases from ~ 0.07 μV/m to ~ 1.2 μV/m, that is about 16 times.

Roughly speaking, for a frequency band $10 - 150$ Hz within the spot of 100 km radius above the FENICS installation the electric field amplitude is $|\mathbf{E}| \sim 0.3 - 1.2$ μV/m. Thus, for typical current $J_0 = 100$ A during FENICS experiments, the 10 Hz emissions can leak into the upper ionosphere with amplitudes up to ~ 30 μV/m. Such magnitudes could be detected by electric sensors on modern LEO satellites. However, any attempt to detect the response in space to FENICS or any other experiment with power lines as controlled source has not been undertaken yet.

Figure 6 shows the amplitude of the B-component excited by ground linear current of different scales at $f = 0.5$ Hz. For the FENICS installation (100 km) the amplitude of the emitted emission above a source reaches $\sim 8 \cdot 10^{-3}$ pT. Thus, to launch artificial Pc1 pulsations (0.5 Hz) with amplitude $|\mathbf{B}| \sim 1$ pT and $|\mathbf{E}| \sim 10$ μV/m in the outer ionosphere it would be necessary to drive the FENICS installation with the current ∼130 A. An installation with a larger scale is more efficient, e.g. the emission from 200 km current is about 2 times larger than from 100 km current.

4.3. Power lines of different lengths

Now we consider how the amplitude of 50-Hz emission in the upper ionosphere varies depending on the linear scale of a power transmission line with an unbalanced current $J_0 =$ 1 A. Comparison of PLE for various line lengths L is given in Figure 7. Just above ($\rho = 0$) very large-scale ($L = 500$ km) line the electric component amplitude reaches $|\mathbf{E}| \simeq 2.7$ μV/m. Upon decrease of the line length the intensity of PLE in the upper ionosphere decreases down to $|\mathbf{E}| \simeq 1.6$ μV/m for $L = 200$ km, $|\mathbf{E}| \simeq 0.8$ μV/m for $L = 100$ km, $|\mathbf{E}| \simeq 0.5$ μV/m for $L = 60$ km, and $|\mathbf{E}| \simeq 0.2$ μV/m for $L = 25$ km. Thus, typical unbalanced current 10 A can produce PLE with amplitude $\sim 8 - 27$ μV/m above large scale (> 100 km) power lines. PLE with amplitudes about few tens of μV/m have been indeed detected by electric sensor onboard DEMETER and Chibis-M satellites (see references in review [*Pilipenko et al.*, 2021]).

5. Discussion

The developed theoretical model predicts that in the upper nightside ionosphere above a 50-80 Hz transmitter with L=60-100 km on a high-resistive ground and driven by 200 A current, the electric component with amplitude up to $\sim 60 - 160$ μV/m may be expected. This modeling result corresponds to the most favorable conditions, when a satellite is exactly above the source. The modeling in [*Fedorov et al.*, 2020] with an infinite source showed a larger absorption of ELF emission in the daytime ionosphere as compared with nighttime conditions. A high conductivity of the underlaying crust also decreases the power emitted into the ionosphere. The same dependencies are expected for a finite-scale source.

The assumption about an infinite line current provides somewhat overestimated maximal effects as compared with a finite length model. For 50-Hz emission the overestimate amounts to ∼6 times for $L = 60$ km, ∼3.7 times for L=100 km, and ∼2 times for L=200 km. Away from the source ($\rho > 200$ km) the difference between the results of both models becomes small.

The developed model has some limitations. The geomagnetic field has been assumed to be vertical. The account for a finite inclination of the geomagnetic field will not modify the results considerably [*Fedorov et al.*, 2021]. The geomagnetic field can provide some guidance of ELF emission, so as a result an equatorward shift of maximum response in the ionosphere to a ground transmitter should be observed.

Interpretation of observations of signals in the frequency range 0.1–20 Hz generated by a horizontal magnetic dipole at large distances along the Earth surface may demand the account for the horizontal inhomogeneity of the Earth-ionosphere waveguide *Ermakova et*

al. [2021, 2022]. However, for the problem of the upward transmission the account for a horizontal inhomogeneity is not important, in our opinion.

ULF waves in the Hz-frequency range (Pc1 pulsations) are of special significance for space physics. Through the wave-particle interactions, electromagnetic ion-cyclotron waves in the Pc1 band can precipitate magnetospheric relativistic electrons into the atmosphere. Thus, intense Pc1 pulsations can suppress the natural or artificial radiation belts. Therefore, the idea to apply the radio heating facilities, e.g., HAARP or Sura, to stimulate the excitation of artificial Pc1 pulsations was actively studied (e.g., see review of *Guo et al.* [2021]). However, this method demands high costs of construction and maintenance of radio-heating facilities. At the same time, in experiments with power transmission lines as controlled sources of ULF/ELF emissions the driving current up to 10^3 A was used [*Boerner*, 1992]. Power line generated artificial signals in the 1 Hz frequency range were detected over distances of more than 1500 km, and such distances were never reported in case of heating experiments [*Ermakova et al.*, 2006]. Our modeling has shown that an installation with scale >100 km and $\geq$100 A current is sufficient under favorable conditions to stimulate emission in the Pc1 band (0.5 Hz) with amplitude $\sim$1 pT and $\sim$ 10 μV/m. Such amplitudes are typical for natural Pc1 signals in the upper ionosphere. Therefore, the FENICS installation at Kola Peninsula at latitude corresponding to the central part of the outer radiation belt can be used as a tool to deplete the relativistic electrons. The use of large decommissioned power lines, where the AC up to 10^3 A can be easily generated, could be a cheap alternative to the radio heating methods.

The modeling results give some support to the puzzling observations of "weekend effect" and "time mark effect" in ground Pc1 activity [*Guglielmi & Zotov*, 2012]. The electric power consumption is known to have peaks around tops of the hour. As a result, the elevated emission in Pc1 band occurring during bursts of transmitted current in power lines may be a trigger for the magnetospheric ion-cyclotron instability.

6. Conclusions

We have numerically estimated the penetration into the realistic ionosphere of ULF/ELF emission from a ground source modeled as a finite-scale linear current. The modeling shows that 10-150 Hz signals from a $60-100$ km length source with current intensity $100-200$ A can be reliably detected by electric sensors onboard the LEO satellites. The modeling confirms that power transmission lines and rail systems can be a source of PLE leaking into the upper ionosphere. Theoretically, decommissioned power lines can be an alternative tool to stimulate Pc1 pulsation activity in the ionosphere - magnetosphere system.

Acknowledgments. The study is supported by the grant 21-77-30010 from the Russian Science Foundation. The IRI model code is distributed by the NASA's Space Physics Data Facility (http://iri.gsfc.nasa.gov).

7. Appendix: Horizontal field components

As a result of solution of the system (9), application of the inverse first order Hankel′s transform and usage of the expressions (5) (transformed into cylindrical coordinates), the

following relationships for the horizontal components of total field are obtained:

$$B_\varrho = \cos\varphi \left(\varrho^{-1}(A_s - B_c) + \mathbb{K}_0[\tilde{B}_c] \right) - \sin\varphi \left(\varrho^{-1}(A_c + B_s) - \mathbb{K}_0[\tilde{B}_s] \right),$$

$$B_\varphi = \cos\varphi \left(\varrho^{-1}(A_c + B_s) - \mathbb{K}_0[\tilde{A}_c] \right) + \sin\varphi \left(\varrho^{-1}(A_s - B_c) - \mathbb{K}_0[\tilde{A}_s] \right),$$

$$e_\varrho = \cos\varphi \left(\varrho^{-1}(\Phi_c + \Psi_s) - \mathbb{K}_0[\tilde{\Phi}_c] \right) + \sin\varphi \left(\varrho^{-1}(\Phi_s - \Psi_c) - \mathbb{K}_0[\tilde{\Phi}_s] \right),$$

$$e_\varphi = \cos\varphi \left(\varrho^{-1}(\Psi_c - \Phi_s) - \mathbb{K}_0[\tilde{\Psi}_c] \right) + \sin\varphi \left(\varrho^{-1}(\Psi_s + \Phi_c) - \mathbb{K}_0[\tilde{\Psi}_s] \right).$$

Here the Hankel′s transforms of the 1-st order $\mathbb{K}_1$ and zero-th order $\mathbb{K}_0$ have been used. Other abbreviations are $A_{c,s} = \mathbb{K}_1[k^{-1}\tilde{A}_{c,s}]$, $B_{c,s} = \mathbb{K}_1[k^{-1}\tilde{B}_{c,s}]$, $\Phi_{c,s} = \mathbb{K}_1[k^{-1}\tilde{\Phi}_{c,s}]$, and $\Psi_{c,s} = \mathbb{K}_1[k^{-1}\tilde{\Psi}_{c,s}]$. The vertical (field-aligned) components are weak and have not been considered.

References

Bannister, P.R., Williams F.J., Dahlvig A.L., & Kraimer W.A. (1974). Wisconsin Test Facility transmitting antenna pattern and steering measurements, *IEEE Trans. Comm., 22(4),* 412–418.

Boerner, D.E. (1992). Controlled source electromagnetic deep sounding: Theory, results and correlation with natural source results, *Surveys in Geophysics, 13,* 435–488.

Belyaev, P.P., Polyakov, S.V., Ermakova, E.N., et al. (2002) First experiments on generation and receiving artificial ULF (0.3–12) Hz emissions at a distance of 1500 km, *Radiophys. Quantum Electron, 46(12),* 135–145.

Bernstain, S.L., Barrouz, M., Evans, D.E., Griffits, E.S., Macneil, D.A., Nissen, Ch.U., Richer, A., White, D.P., & Willim, D.K. (1974). Distant Communication on Extremely Low Frequencies, *Proceedings IEEE, 62,* 5–30.

Budden, K.G. (1985). The propagation of radio waves, Cambridge University Press.

Ermakova, E.N., Kotik, D.S., Polyakov, S.V., Bosinger, T., & Sobchakov, L.A. (2006). A power line as a tunable ULF-wave radiator: Properties of artificial signal at distances of 200 to 1000 km, *Journal Geophysical Research, 111,* doi:10.1029/2005JA011420.

Ermakova, E.N., Ryabov, A.V., & Kotik, D.S. (2021). Features of the spectra of ultralow-frequency magnetic fields from horizontal current sources: models of plane and spherical waveguides Earth-ionosphere, *Radiophys. Quantum Electron. 64,* N3, 163-178.

Ermakova, E.N., Kotik, D.S., & Ryabov, A.V. (2022). Characteristics of ULF magnetic fields in the 3D inhomogeneous Earth-ionosphere waveguide, *J. Geophys. Res., 127,* e2021JA030025. doi:10.1029/2021JA030025

Fedorov, E., Mazur, N., Pilipenko V., & Baddeley, L. (2016). Modeling the high-latitude ground response to the excitation of the ionospheric MHD modes by atmospheric electric discharge, *Journal Geophysical Research: Space Physics, 121,* doi:10.1002/2016JA023354.

Fedorov, E., Mazur, N., Pilipenko V., & Vakhnina, V. (2020). Modeling ELF electromagnetic field in the upper ionosphere from power transmission lines, *Radio Science, 121,* 55, e2019RS006943, doi:10.1029/2019RS006943.

Fedorov E.N., Mazur N.G., & Pilipenko V.A. (2021). Electromagnetic response of the mid-latitude ionosphere to power transmission lines. *Journal of Geophysical Research: Space Physics, 126,* e2021JA029659. https://doi.org/10.1029/2021JA029659.

Fedorov, E.N., Mazur, N.G., & Pilipenko, V.A. (2022). Electromagnetic field in the upper ionosphere from horizontal ELF ground-based transmitter with a finite length, *Radiophys. Quantum Electron., 64*

Fraser-Smith, A.C., & Coates, D.B. (1978). Large-amplitude ULF electromagnetic fields from BART, *Radio Sci., 13,* 661–668, doi:10.1029/RS013i004p00661.

Guglielmi, A.V., & Zotov, O.D. (2012). The phenomenon of synchronism in the magnetosphere-technosphere-lithosphere dynamical system, *Physics of the Solid Earth, 48(6),* doi:10.1134/S1069351312050035.

Guo, Z., Fang, H., & Honary, F. (2021) The Generation of ULF/ELF/VLF waves in the ionosphere by modulated heating. *Universe, 7,* 29. doi:10.3390/universe7020029.

Inan, U.S., Cummer, S.A., & Marshall, R.A. (2010). A survey of ELF and VLF research on lightning-ionosphere interactions and causative discharges, *Journal of Geophysical Research, 115*, A00E36, doi:10.1029/2009JA014775.

Kostrov, A.V., Gushchin, M.E., & Strikovskii, A.V. (2017). Generation and radiation of high power line harmonics, *Geomagnetism and Aeronomy, 57*, 482–490, doi:10.1134/S0016793217030094.

Mazur, N.G., Fedorov, E.N., Pilipenko, V.A., & Vakhnina, V.V. (2018). ULF electromagnetic field in the upper ionosphere excited by lightning. *Journal of Geophysical Research: Space Physics, 123,* 6692–6702. doi:10.1029/2018JA025622.

Nemec, F., Santolik, O., Parrot, M., & Bortnik, J. (2008). Power line harmonic radiation observed by satellite: Properties and propagation through the ionosphere, *Journal of Geophysical Research, 113,* A08317.

Nemec, F., Parrot, M., & Santolik, O. (2015). Power line harmonic radiation observed by the DEMETER spacecraft at 50/60 Hz and low harmonics, *Journal Geophysical Research: Space Physics, 120,* 8954–8967.

Nickolaenko, A.P., Shvets, A.V., & Hayakawa, M. (2016). Extremely Low Frequency (ELF) radio wave propagation: a Review, *International Journal of Electronics and Applied Research, 3(2)*, 81 pp. (http://eses.co.in)

Parrot, M. (2018). DEMETER observations of manmade waves that propagate in the ionosphere, *Comptes Rendus Physique, 19,* 26–35. doi: 10.1016/j.crhy.2018.02.001

Pilipenko, V.A., Parrot, M., Fedorov, E.N., & Mazur, N.G. (2019). Electromagnetic field in the upper ionosphere from ELF ground-based transmitter, *Journal of Geophysical Research: Space Physics, 124*, doi: 10.1029/2019JA026929.

Pilipenko, V.A., Fedorov, E.N., Mazur, N.G., & Klimov, S.I. (2021). Electromagnetic "pollution" of near-earth space by radiation from power lines. *Solar-Terrestrial Physics, 7,* N3. 3–12. doi: 10.12737/szf-71202101.

Pilipenko, V.A. (2021) Space weather impact on ground-based technological systems. *Solar-Terrestrial Physics, 7,* N3, 68–104, DOI:10.12737/stp-73202106.

Rothkaehl, H. & Parrot, M. (2005). Electromagnetic emissions detected in the topside ionosphere related to the human activity, *Journal of Atmospheric Solar-Terrestrial Physics, 67,* 821–828.

Sobchakov, L.A. Astakhova, N.L., & Polyakov, S.V. (2003). Excitation of electromagnetic waves in a plane waveguide with an anisotropic upper wall, *Radiophys. Quantum Electron, 46(12),* 918–927.

Starks, M.J., Quinn, R.A., Ginet, G.P., Albert, J.M., Sales, G.S., Reinisch, B.W., & Song, P. (2008). Illumination of the plasmasphere by terrestrial very low frequency transmitters: Model validation, *Journal Geophysical Research, 113,* A09320, doi:10.1029/2008JA013112.

Tereshenko, E.D., & Tereshenko, P.E. (2017). Electric field of horizontal linear water-grounded aerial, *Journal of Technical Physics, 87,* 453–457.

Velikhov, Ye.P., Zhamaletdinov, A.A., Sobchakov, L.A., Veshev, A.V., Saraev, A.K., Tokarev, A.D., Shevtsov, A.N., Vasiljev, A.V., Sonnikov, A.G., & Yakovlev, A.V. (1994). Experiment on the frequency electromagnetic sounding of the Earth Crust with the use of the powerful ELF antenna, *Doklady Akademii Nauk. 338.* N1. 106–109.

Velikhov, E.P., Zhamaletdinov, A.A., Shvetsov, A.N., Tokarev, A.D., Kononov, Yu.M., Pesin, L.B., Kadyshevich, G.M., Pertel, M.I., & Veshchev A.V. (1998), Deep electromagnetic studies with the use of powerful ELF radio intallations, *Physics of the Solid Earth, 34,* N8, 615–632.

Wait, J.R. (1972), Electromagnetic Waves in Stratified Media, 372 pp., Elsevier, New York.

Wu, J., Fu, J.J., & Zhang, C. (2014). Propagation characteristics of power line harmonic radiation in the ionosphere, *Chinese Physics B., 23*, 034,102–034,107, doi:10.1088/1674-1056/23/3/034102.

Wu, J., Guo, Q., Yan, X. & Zhang C. (2019a). Theoretical analysis on affecting factors of power line harmonic radiation, *IEEE Transactions on Plasma Science, 47,* 770-775, doi:10.1109/TPS.2018.2865827.

Wu, J., Guo, Q., Yue, C., Xie, L., & Zhang, C. (2019b). Special electromagnetic interference in the ionosphere directly correlated with power system, *IEEE Transactions on Electromagnetic Compatibility*, doi:10.1109/TEMC.2019.2918280.

Zhamaletdinov, A.A., Shevtsov, A.N., Velikhov, E.P., et al. (2015). Study of interaction of ELF-ULF range (0.1-200 Hz) electromagnetic waves with the Earth's crust and the iono-

sphere in the field of industrial power transmission lines (FENICS experiment), *Izvestiya - Atmospheric and Oceanic Physics, 51,* 826–857.

Zhang, C. & Ma, Q. (2018). Influences of radiation from terrestrial power sources on the ionosphere above China based on satellite observation, *2nd International Workshop on Renewable Energy and Development, Conf. Series: Earth and Environmental Science 153,* 042002, doi:10.1088/1755-1315/153/4/042002.

Figure 1. Sketch of the problem geometry.

Figure 2. The magnitudes of the total horizontal electric component $|E|$ of electromagnetic emission at altitude $z = 660$ km generated by a line current oscillator at $f = 82$ Hz with $J_0 = 1$ A and lengths $L = 60$ km and $L = 500$ km in the upper nighttime ionosphere.

Figure 3. The magnitude of the total horizontal magnetic field $|B|$ of electromagnetic emission generated by a ground 82 Hz transmitter with length $L = 60$ km and $J_0 = 1$ A.

Figure 4. The ZEVS radiation pattern in the upper ionosphere for the electric component

Figure 5. The ELF emission intensity in the upper ionosphere ($z = 660$ km) above the FENICS installation ($L = 100$ km) for various emission frequencies.

Figure 6. The amplitude of the B-component excited by ground linear currents of different scales at $f = 0.5$ Hz.

Figure 7. The amplitude of 50-Hz emission in the upper ionosphere for different linear scales of power transmission line with unbalanced current $J_0 = 1$ A.

Figure 1.

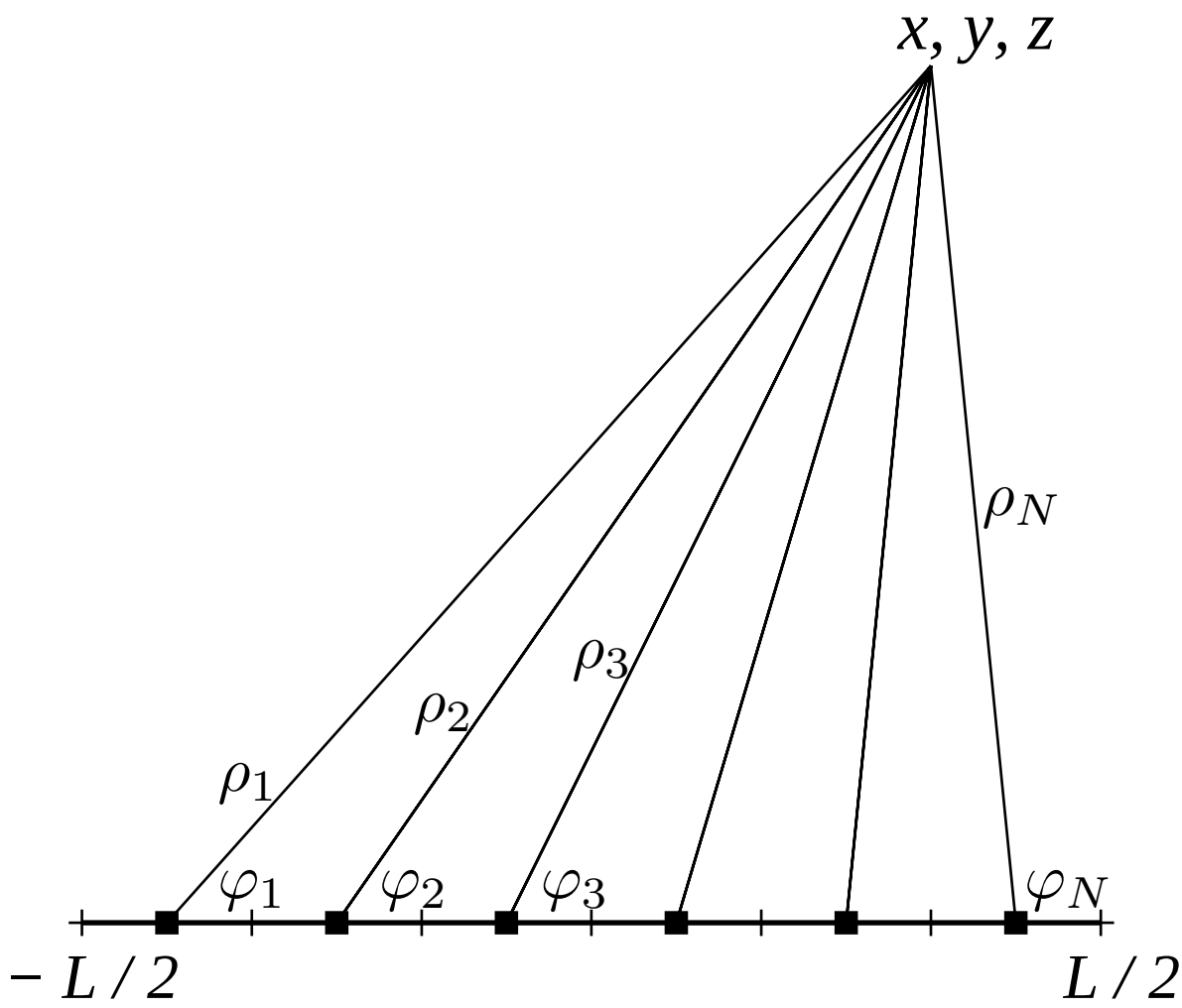
x, y, z
ρ1
ρ2
ρ3
ρN
φ1
φ2
φ3
φN
− L / 2
L / 2

Figure 2.

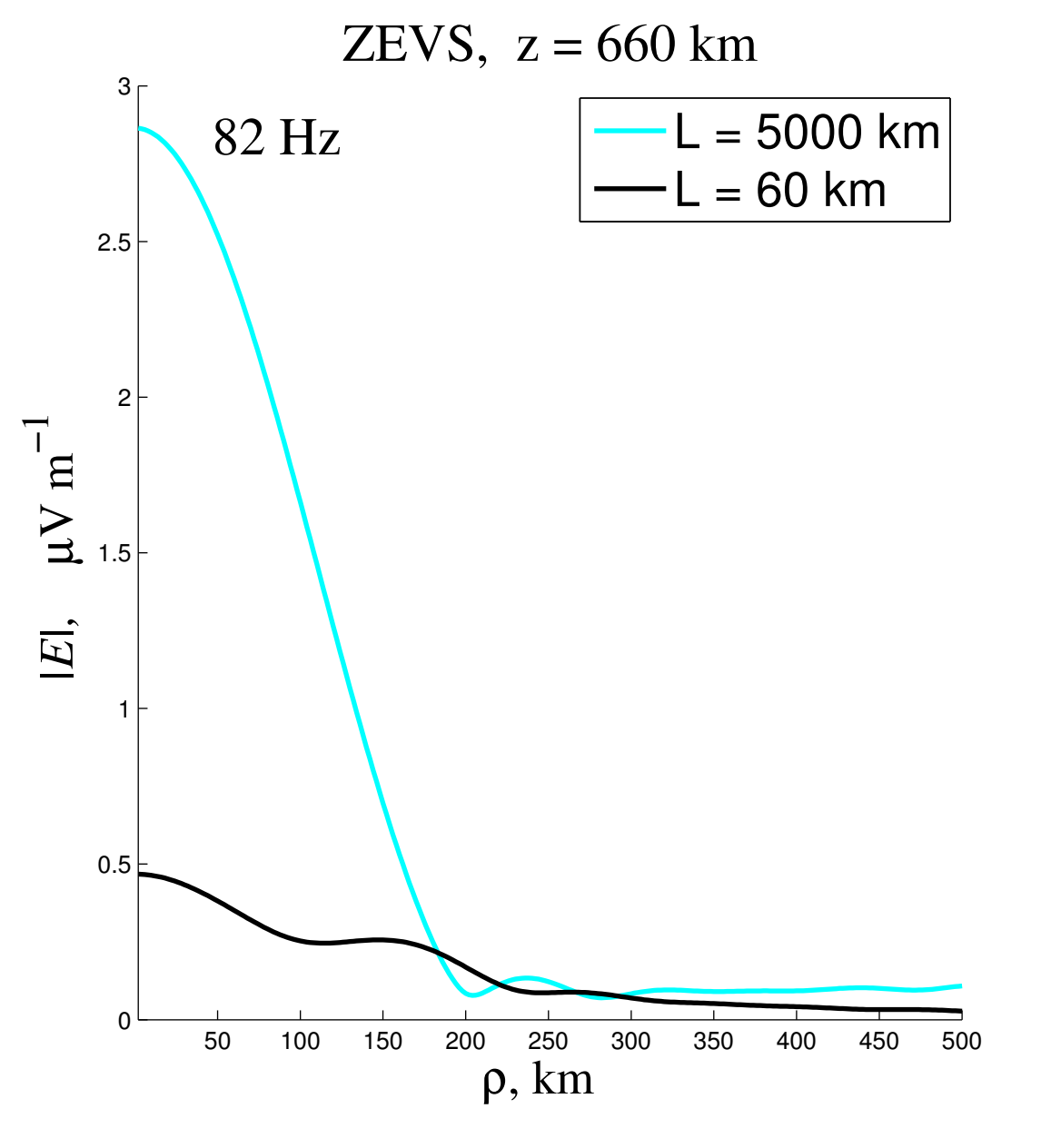
ZEVS, z = 660 km
82 Hz
L = 5000 km
L = 60 km
|E|, μV m−1
ρ, km
0
0.5
1
1.5
2
2.5
3
50
100
150
200
250
300
350
400
450
500

Figure 3.

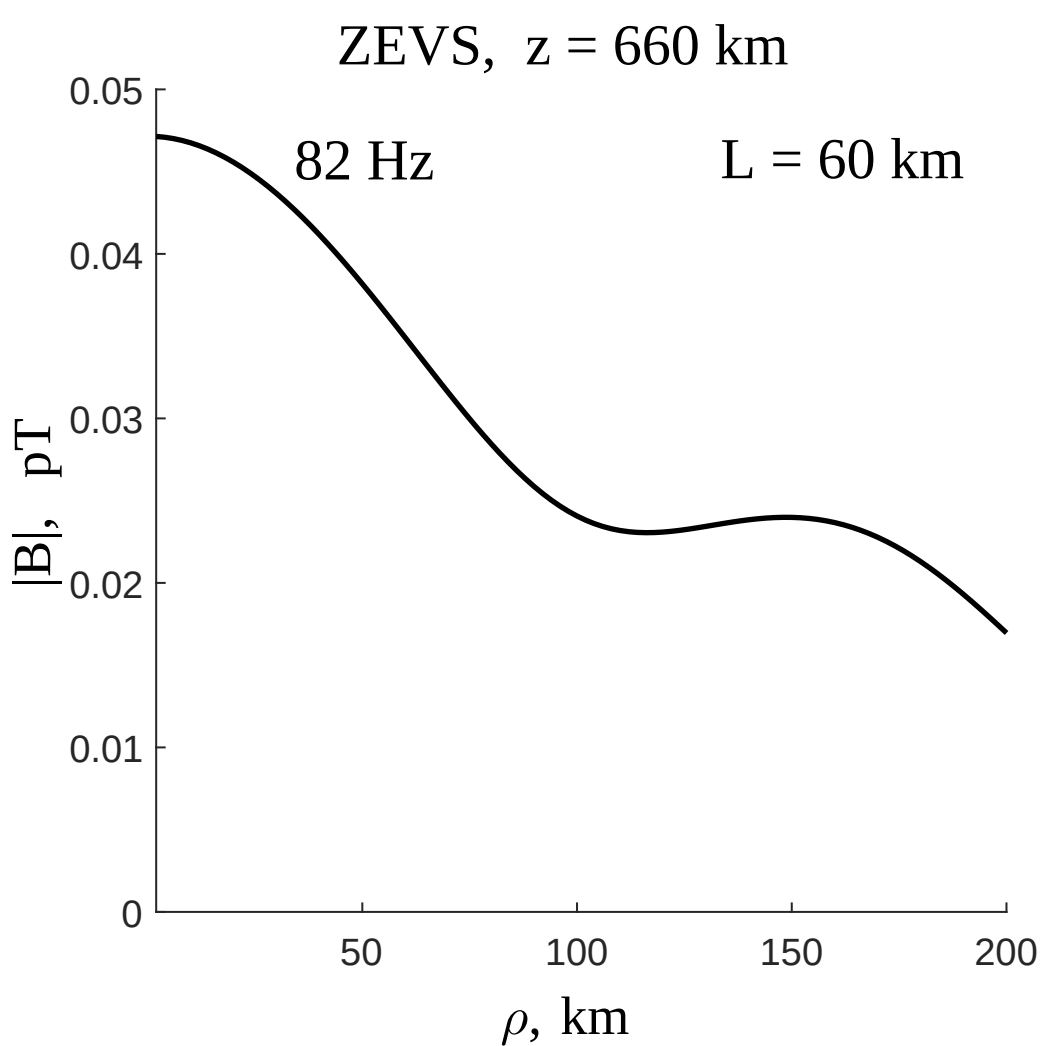
ZEVS, z = 660 km
82 Hz
L = 60 km
|B|, pT
0.05
0.04
0.03
0.02
0.01
0
50
100
150
200
ρ, km

Figure 4.

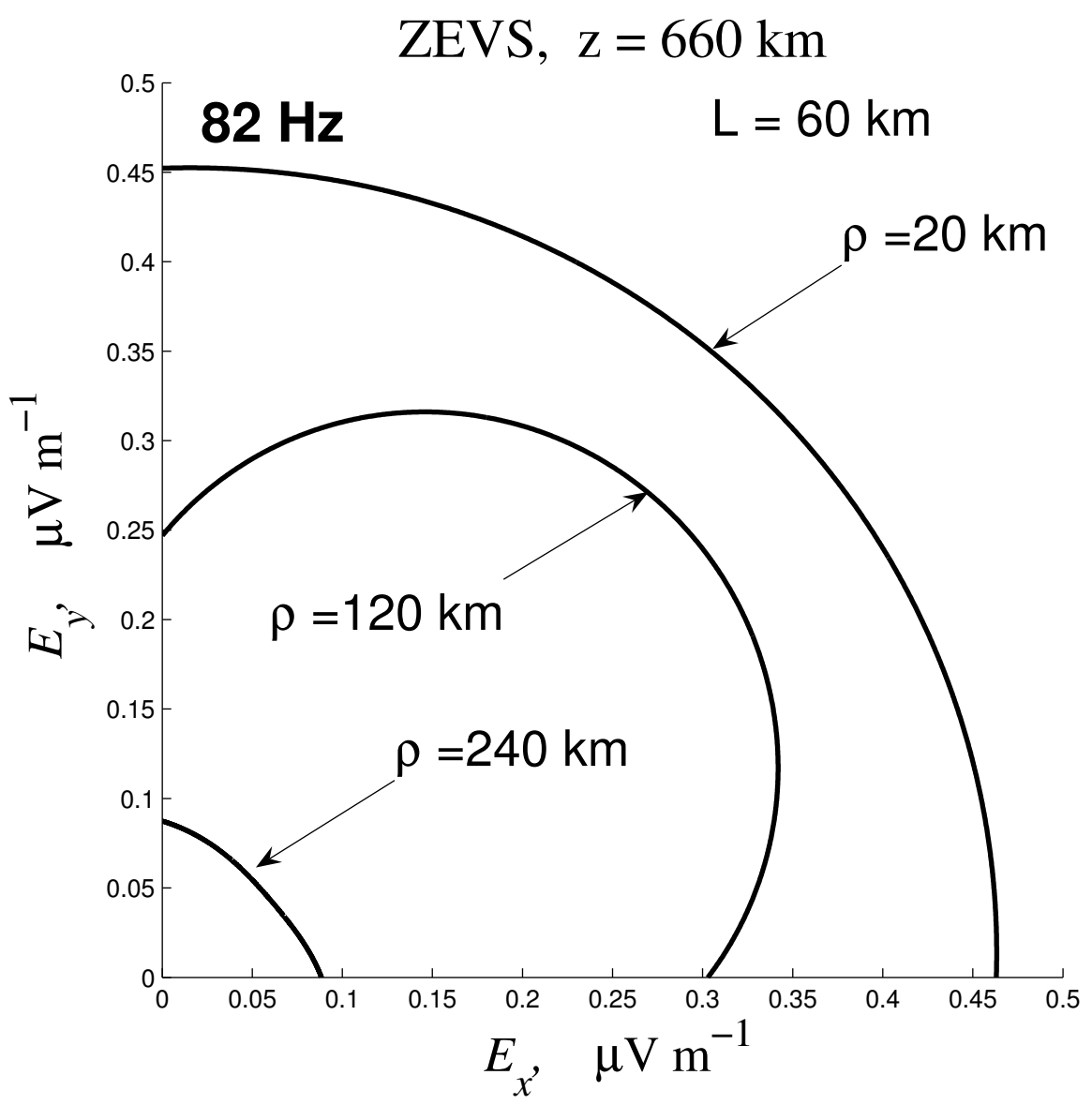
ZEVS, z = 660 km
82 Hz
L = 60 km
ρ =20 km
ρ =120 km
ρ =240 km
E_y, μV m^{-1}
E_x, μV m^{-1}
0
0.05
0.1
0.15
0.2
0.25
0.3
0.35
0.4
0.45
0.5

Figure 5.

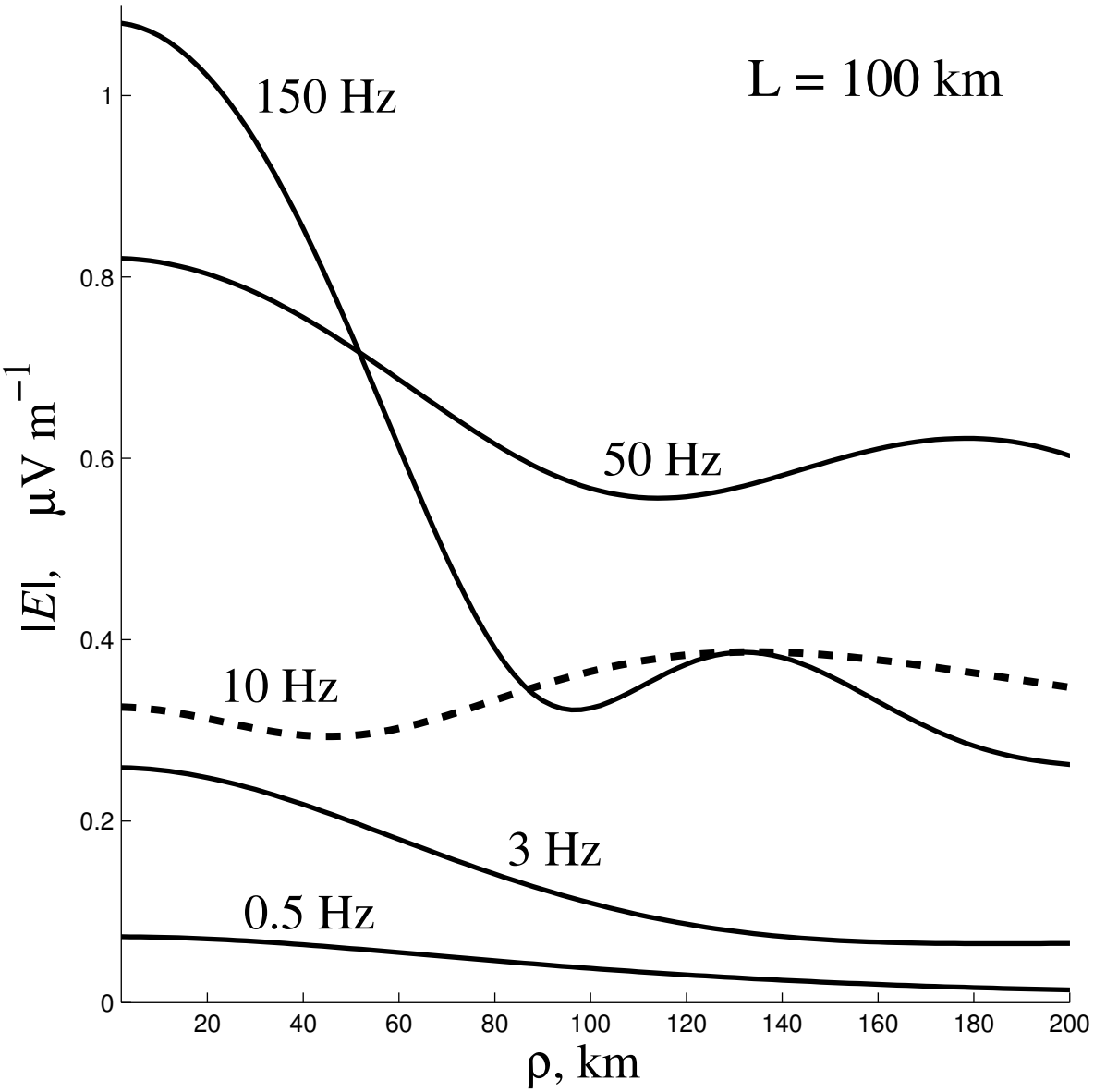
FENICS, z = 660 km
L = 100 km
150 Hz
50 Hz
10 Hz
3 Hz
0.5 Hz
|E|, μV m−1
ρ, km
0
0.2
0.4
0.6
0.8
1
20
40
60
80
100
120
140
160
180
200

Figure 6.

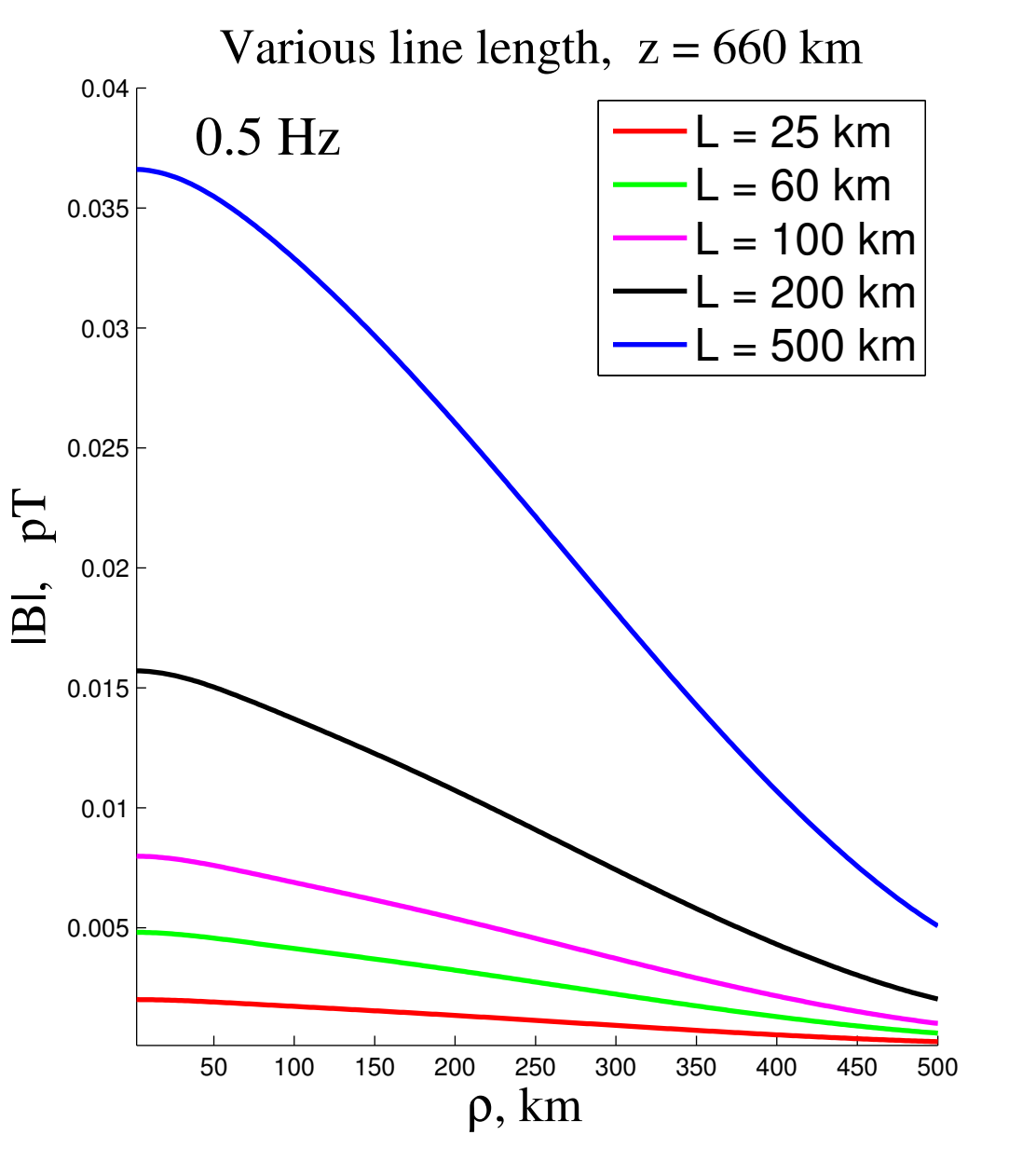
Various line length, z = 660 km
0.5 Hz
L = 25 km
L = 60 km
L = 100 km
L = 200 km
L = 500 km
|Bl, pT
0.04
0.035
0.03
0.025
0.02
0.015
0.01
0.005
50
100
150
200
250
300
350
400
450
500
ρ, km

Figure 7.

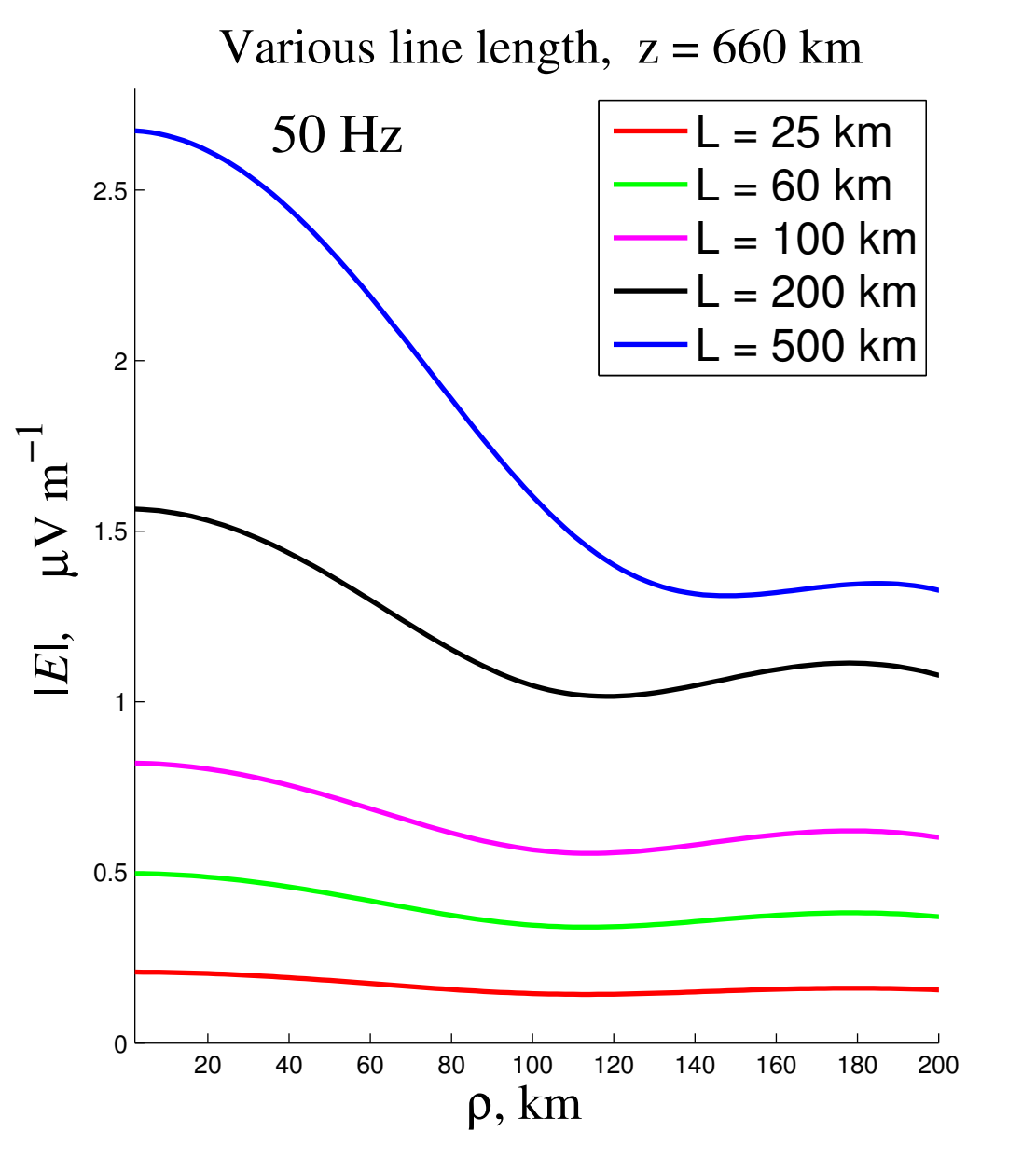
Various line length, z = 660 km
50 Hz
L = 25 km
L = 60 km
L = 100 km
L = 200 km
L = 500 km
|E|, μV m−1
ρ, km
0
0.5
1
1.5
2
2.5
20
40
60
80
100
120
140
160
180
200